Available online at www.sciencedirect.com
ScienceDirect
Tetrahedron
Tetrahedron 63 (2007) 1617–1623

Design and synthesis of squaraine based near infrared fluorescent probes

M. C. Basheer,[a] U. Santhosh,[a] S. Alex,[a] K. George Thomas,[a] Cherumuttathu H. Suresh[b] and Suresh Das[a,*]

[a]*Photosciences and Photonics Section, Chemical Sciences and Technology Division, Regional Research Laboratory (CSIR), Trivandrum-695 019, Kerala, India*
[b]*Computational Modeling and Simulation Section, Regional Research Laboratory (CSIR), Trivandrum-695 019, Kerala, India*

Received 22 August 2006; revised 22 November 2006; accepted 7 December 2006
Available online 8 January 2007

Abstract—A novel class of dialkylanthracene containing squaraine dyes (**Sq1**–**3**) possessing intense absorption and emission in the NIR region has been synthesized. Structural and electronic features investigated using DFT methods suggest that the significant bathochromic shifts observed on replacing dialkylaniline by dialkylanthracene in this class of molecules can be attributed to a reduction in the HOMO–LUMO gap mainly due to enhanced hydrogen bonding between the carbonyl group of the cyclobutane ring and the neighboring aromatic hydrogen in the dyes containing the anthracene moiety. The absence of fluorescence in aqueous media and high fluorescence when encapsulated into hydrophobic domains make this class of dyes especially useful as probes for mapping such domains in biological systems.

1. Introduction

The development of new dyes with strong emission in the near infrared (NIR) region (700–900 nm) plays a crucial role in advancing techniques for noninvasive monitoring of diseased tissues.[1] Cells excited at wavelengths below 500 nm produce considerable autofluorescence mainly from flavins, flavoproteins, and NADH, which can very often swamp the probe fluorescence. This aspect combined with greater tissue penetration and reduced photochemical damage of cells makes fluorescence microscopy in the NIR region especially attractive for biomedical applications.[2] The limited number of photostable fluorochromes with strong emission in the NIR region on the other hand, forms a major bottleneck in the use of fluorescence microscopy.

Squaraines form a class of dyes with intense absorption in the red to near infrared region.[3] Their unique photochemical and photophysical properties[4] make them useful in a variety of applications such as in copiers,[5] solar cells,[6] optical discs,[7] and sensors.[8] Squarylium dyes with tertiary arylamine end groups are known to possess better stability and solubility than those with heterocyclic end groups.[3b,9] However, dyes in this class with absorbance maxima beyond 700 nm are limited.[9a,10] Our continued efforts to develop strongly luminescent NIR dyes led us to the synthesis of a novel class of tertiary arylamine derivatives (**Sq1**–**3**, Fig. 1).

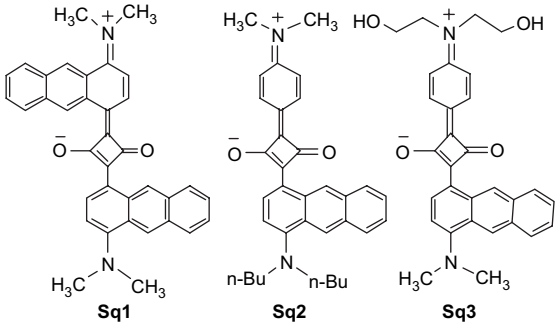

Figure 1.

2. Results and discussion

2.1. Synthesis

Several modes of addition of squaric acid to the dimethyl aminoanthracene ring are possible (see Supplementary data). On heating *N*,*N*-dimethyl-1-aminoanthracene (**DMA**) and squaric acid at 120 °C for 12 h in *n*-butanol/toluene, however, only a single product with an absorption maximum centered around 800 nm was formed (Scheme 1).[11]

Keywords: Near infrared dyes; Squaraine; Fluorescent probes; Micelles; Modeling.
* Corresponding author. Tel.: +91 471 2515318; fax: +91 471 2491712; e-mail: sdaas@rediffmail.com

0040–4020/$ - see front matter © 2007 Elsevier Ltd. All rights reserved.
doi:10.1016/j.tet.2006.12.007

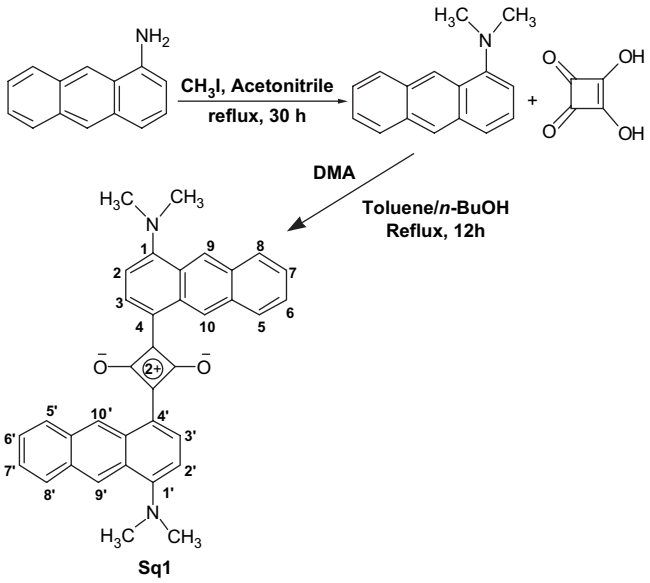

Scheme 1.

Detailed 2D NMR studies have been carried out to characterize the structure of the product formed. The ^{1}H NMR spectra (500 MHz) showed four doublets, two triplets, two singlets in the aromatic region (6.5–10.7 ppm), and a singlet at 3.39 ppm corresponding to $N(CH_3)_2$ protons indicating a symmetrical structure. Formation of a symmetrical dye through coupling of squaric acid at C-9 or C-10 position was ruled out due to the presence of two singlet peaks in the aromatic region. All the protons in the aromatic region were further established by ^{1}H–^{1}H COSY and ^{1}H–^{1}H ROESY experiments. It was observed that the doublets at 7.00 and 9.57 ppm were mutually coupled in ^{1}H–^{1}H COSY experiments (Fig. 2). The spatial interaction was observed between the $N(CH_3)_2$ protons and the doublet at 7.00 ppm as well as the singlet at 8.60 ppm in ^{1}H–^{1}H ROESY experiments (see Supplementary data). By comparing the 2D NMR spectra the doublet at 7.00 ppm is attributed to C-2 proton, the doublet at 9.57 ppm to C-3 proton, and the singlet at 8.60 ppm to the C-9 proton. Similarly, it was observed from ^{1}H–^{1}H COSY experiment that the triplet at 7.53 ppm (C-7) was coupled with the doublet at 7.99 ppm (C-8) and the triplet at 7.59 ppm (C-6) was coupled with the doublet at 8.34 ppm (C-5) (Fig. 2). These studies further confirm that the addition of squaric acid occurs through 4,4′-positions of **DMA**, resulting in the formation of the dye shown in Scheme 1.

The unsymmetrical squaraine dyes, **Sq2** and **Sq3**, were synthesized by the condensation of 3-[4-(*N*,*N*-dialkylamino)anthracene]-4-hydroxy-cyclobutene-1,2-dione with the appropriate dialkylanilines. The dihydroxyethanolamine moiety at the terminal position of **Sq3**, made this dye water compatible, which is an essential requirement for biological applications.

2.2. Absorption and fluorescence properties

Figure 3 shows the absorption and emission spectra of **Sq1** and **Sq2** along with that of bis[4-(*N*,*N*-dibutylamino)phenyl]squaraine (**DBAS**).[12] The photophysical properties of these dyes in toluene and ethanol are summarized in Table 1.

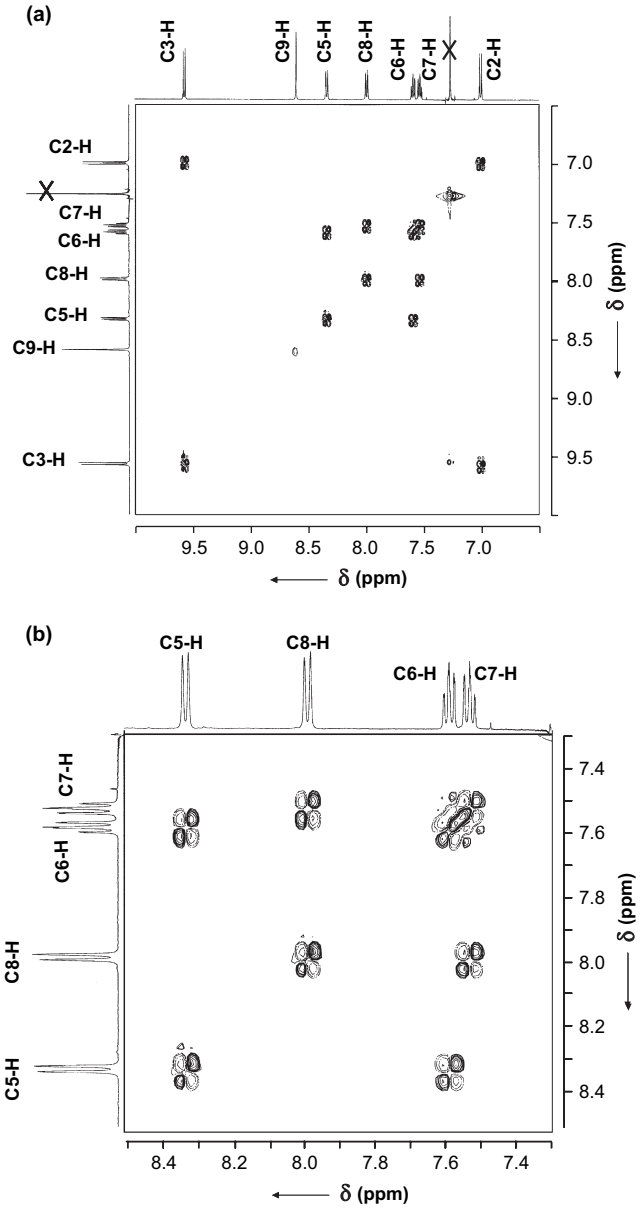

Figure 2. ^{1}H–^{1}H COSY spectrum of **Sq1** (a) 6.5–10 ppm, (b) 7.3–8.5 ppm.

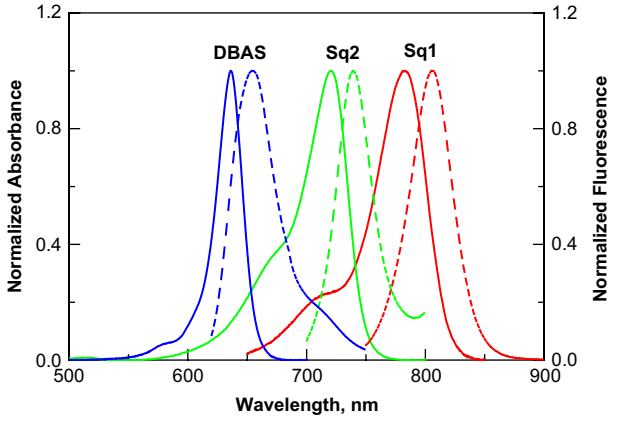

Figure 3. Normalized absorption (solid line) and emission spectra (dashed line) of **Sq1**, **Sq2**, and **DBAS** in toluene.

Table 1. Absorption and emission maxima, quantum yields of fluorescence, and lifetimes of **Sq1**, **Sq2**, and **Sq3** in toluene and ethanol

	Toluene				Ethanol			
	λ_{max} (nm)		Φ_f[b]	τ_f, ns	λ_{max} (nm)		Φ_f[b]	τ_f, ns
	Abs	Em			Abs	Em		
Sq1	782	805	0.24	1.5	789	811	0.03	0.20
Sq2	720	739	0.30	2.2	726	749	0.05	0.50
Sq3	[a]	[a]	[a]	[a]	720	743	0.06	0.40

[a] **Sq3** is insoluble in toluene.
[b] Quantum yield was determined by using **DDI** (1,1′-diethyl-2,2′-dicarbocyanine iodide) Φ_{EtOH}=0.0028[14] (for **Sq2** and **Sq3**) and **IR-125** Φ_{DMSO}=0.13[13c] (for **Sq1**) as standard, error ca. ±5%.

Replacement of each dialkylamino phenyl group with a dialkylamino anthracene moiety results in a significant red shift in the absorption and emission bands of the dyes. Thus, an 80 nm shift was observed between the absorption maximum of **DBAS** and **Sq2**, while the shift was nearly 140 nm between that of **DBAS** and **Sq1**. These dyes possessed fairly high quantum yields of fluorescence, better than or comparable to some of the best dyes reported with absorption and emission in the NIR region.[13] The fluorescence quantum yields and lifetimes of **Sq1** and **Sq2** were much higher in toluene than in ethanol.

2.3. Photophysical properties in aqueous and micellar media

The water compatibility of **Sq3** was investigated by studying its absorption and emission properties in ethanol/water solvent mixtures (Table 2). Increasing the water content resulted in a blue shift, broadening and reduction in intensity of the absorption band. This was accompanied by a significant decrease in the emission intensity. These effects could be attributed to the formation of aggregates[15] as well as hydrogen-bonding interactions with water.[16] The photostability of the dyes under these conditions was ascertained by the lack of change in their absorption and emission spectra in ethanol/water on extended irradiation (>4 h) with 690 nm light from the 450 W excitation lamp of the SPEX-Fluorolog.

In biological systems the dyes can encounter hydrophobic environments marked by much higher viscosity, lower dielectric constant and polarity, and poorer hydrogen bond donor capabilities, compared with that of free solutions. Investigation of the photophysical properties in micellar media, which can mimic some of these conditions, can provide useful information on the behavior of the dyes in such environments. In view of this, the absorption and fluorescence properties of **Sq3** were examined in the presence of cetyltrimethylammonium bromide (CTAB), sodium dodecyl sulfate (SDS), and polyethylene-*tert*-octylphenol (Triton X-100). Figure 4 shows the effect of SDS on the absorption spectrum of **Sq3** in 96% (v/v) water/ethanol. On addition of SDS a bathochromic shift and an increase in the intensity of absorption were observed. This can be attributed to the break-up of the aggregate and recovery of the monomer. The absorption changes were accompanied by a significant enhancement in fluorescence yield (inset, Fig. 4, Table 2). The increase in fluorescence intensity can be attributed to microencapsulation of the dye into the hydrophobic interior of the micelle. Maximum enhancement of fluorescence was observed above the critical micelle concentration (CMC), which is 8.0 mM for SDS. Similar observations were made for the cationic micelle CTAB and the nonionic micelle Triton X-100 (see Supplementary data). The enhancement in fluorescence lifetime in the presence of micelles is clearly observable from Figure 5. These effects can be attributed to microencapsulation of the dye within the hydrophobic

Table 2. Absorption/emission maxima, quantum yield of fluorescence, and lifetimes of **Sq3** in water/ethanol binary mixtures and surfactant solutions

Solvent %H_2O[a]	λ_{max} (nm)		Φ_f[b]	τ_f, ns
	Abs	Em		
20	720	754	0.06	0.30
80	711	749	0.013	0.20
96	704	735	0.004	0.05
96+CTAB[c]	727	753	0.09	1.06
SDS[c]	719	747	0.075	0.60
Triton X-100[c]	731	755	0.155	1.33

[a] Binary mixture containing water and ethanol.
[b] Quantum yield determined by using **DDI** as standard (Φ_f=0.0028 in EtOH), error ca. ±5%, λ_{ex}=690 nm.
[c] CTAB 1.5 mM, SDS 9.2 mM, and Triton X-100 2.1 mM.

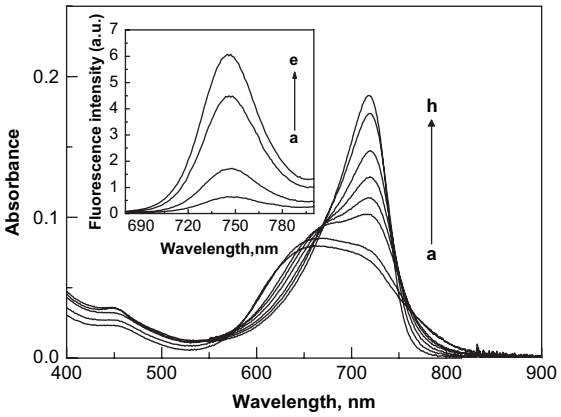

Figure 4. Effect of SDS on absorption properties of **Sq3** [2.43×10^{-5} M] in 96% (v/v) water/ethanol mixture. [SDS] (a) 0, (b) 0.28, (c) 0.83, (d) 1.39, (e) 1.95, (f) 2.5, (g) 3.1, and (h) 9.2 mM. Inset shows the effect of addition of SDS on the fluorescence spectrum of **Sq3**. [SDS] (a) 0, (b) 1.95, (c) 2.5, (d) 3.1, and (e) 9.2 mM, λ_{ex}=662 nm.

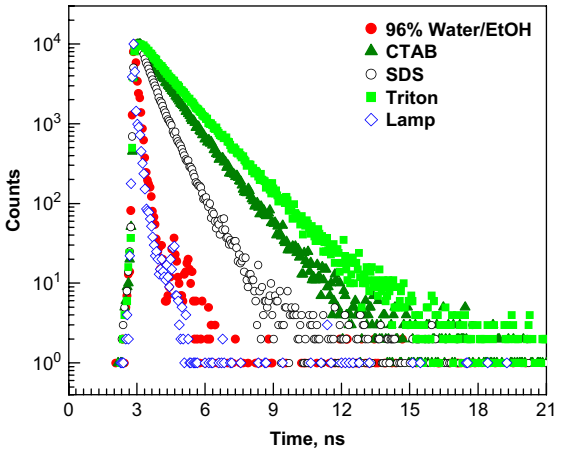

Figure 5. Fluorescent decay profile of **Sq3** in 96 % (v/v) water–ethanol mixture, 1.5 mM CTAB, 9.2 mM SDS, and 2.1 mM Triton. Lamp profile is also shown. Emission wavelength monitored at 750 nm, λ_{ex}=635 nm.

micellar cavity.[13c,17] The absence of fluorescence in aqueous media and high fluorescence when encapsulated into hydrophobic domains make this dye specially useful as a probe for mapping such domains in biological systems.[17,18]

2.4. Molecular modeling of the complexes at the DFT and semi empirical PM3 levels

The most common strategy used for shifting the absorption band of the chromophoric system to the NIR region is to extend the conjugation between the terminal groups.[19] Such an approach, however, has its own limitations as in the case of some cyanine and related linear dye systems, which undergo symmetry collapse and bond localization at long chain lengths. Increased conjugation between terminal groups is also known to result in a reduction in the photo- and thermal stability of the dyes. The present study shows that the use of dialkyl aminoanthracene instead of dialkylanilines can provide a facile strategy for obtaining squaraine dyes with increasingly red shifted absorption and emission.

In order to understand the structural and electronic features of the systems, the solution phase geometries in ethanol were optimized for **DBAS**, **Sq1**, and **Sq2** at BLYP/6-31G* level of density functional theory in conjunction with the polarizable continuum (PCM) model of Tomasi and co-workers (Fig. 6).[20,21] The Gaussian 03 suite of programs were used for the calculations.[22]

In **DBAS** and **Sq2**, the dimethyl amino group is coplanar with the phenyl moiety whereas a twist angle of 17° was observed between this group and the anthracene moiety in **Sq1** and **Sq2**. Further, the CN bond lengths in the range of 1.376–1.398 Å observed in these systems are much shorter than a typical CN single bond length of 1.48 Å, indicating a partial double bond character and partial positive charge on the nitrogen. This can be attributed mainly to the strong electron donating mesomeric effect of the nitrogen lone pair. The CO bond lengths in the range of 1.250–1.252 Å observed in these systems are much longer than the typical value of 1.22 Å, indicative of an anionic C–O$^-$ character. The anionic nature of the CO facilitates the interaction with the nearby CH bonds on the aromatic moiety (see the CO···HC nonbonded interaction shown in Fig. 5 by dotted lines). In addition, the structural restrictions imposed by the middle ring of the anthracene moiety in **Sq1** and **Sq2** bring the CO oxygen and CH bonds into close proximity making it favorable for the CO···HC interactions. Thus, the shortest CO···HC length is observed in **Sq1** (2.073 Å) and **Sq2** (2.061 Å). All the CO···HC interactions could be characterized as hydrogen bonds since they showed (3, −1) bond critical points in the Bader's atoms in molecule (AIM) analysis.[23] The electron density at the critical points was found to increase with the decrease in the CO···HC bond distances, suggesting maximum hydrogen bond interactions in **Sq1** (see Supplementary data for AIM details).

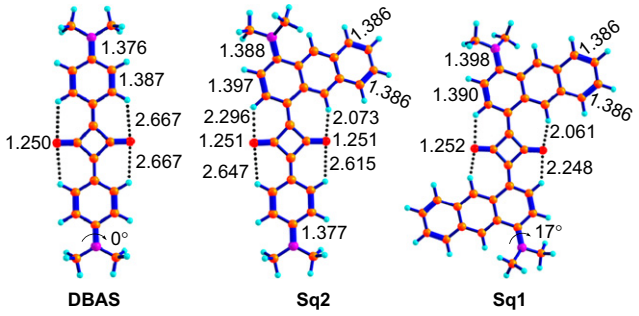

Figure 6. Optimized geometries of **DBAS**, **Sq1**, and **Sq2** at BLYP/6-31G*-PCM level. Important bond lengths in angstrom are also given. Bond lengths below 1.400 Å are shown in thick lines.

In Figure 7, the molecular electrostatic potential (MESP) plotted on the van der Waals' surface of **Sq1** illustrates the highly charge separated (zwitterionic) character of the system.[8a,24,25] As expected, the positive MESP is largely localized on the dimethyl amino group (red region) while the negative MESP is mainly on the squaraine oxygens (blue region). This feature of MESP was also observed in **DBAS** and **Sq2** (see Supplementary data).

The absorption properties of the systems optimized at BLYP/6-31G*-PCM level were further analyzed using time-dependent DFT (TDDFT) calculations.[26] The calculated λ_{max}, oscillator strength, and the main MO transitions are provided in Table 3. The calculated λ_{max} values are in good agreement with the experimental values. In all the cases, the main MO transition corresponding to the NIR absorption is from HOMO to LUMO. The HOMO is delocalized over the entire molecule while the LUMO shows more localization on the arene ring directly connected to the squaraine moiety and two of the squaraine carbon atoms (Fig. 8a). The HOMO–LUMO gap (Fig. 8b) shows a gradual decrease when going from **DBAS** to **Sq2** to **Sq1**, which correlates well with the observed bathochromic shift.

The structural and electronic features suggest extended π-conjugation in **Sq1** and **Sq2** via the anthracene moiety and

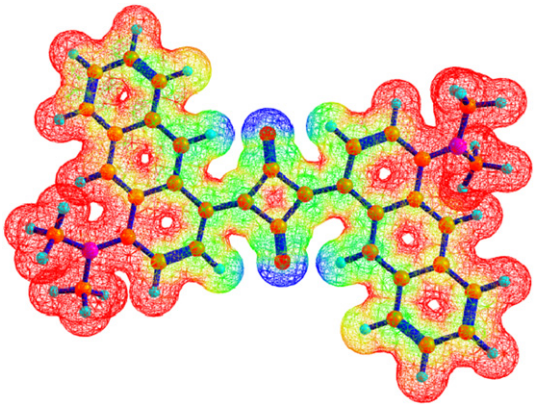

Figure 7. Molecular electrostatic potential mapped onto the van der Waals' surface of **Sq1**. Color coding ( ) red to blue is +44 to −31 kcal/mol.

Table 3. Calculated absorption TDDFT at BLYP/6-31G*-PCM level wavelengths in nanometer and oscillator strengths

System	λ_{max}, nm	f	MO transition
Sq1	786	1.0884	HOMO to LUMO (54%)
Sq2	704	1.0355	HOMO to LUMO (53%)
DBAS	591	1.6401	HOMO to LUMO (56%)

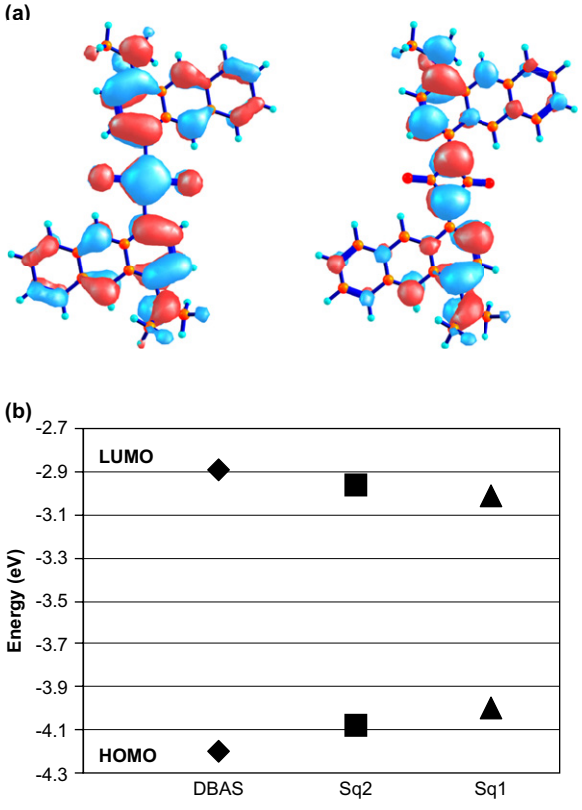

Figure 8. (a) HOMO and LUMO of **Sq1** and (b) HOMO–LUMO gap in **DBAS**, **Sq1**, and **Sq2**.

strong mesomeric effect of the dimethyl amino group. The CO···HC hydrogen bond interaction further enhances the electron delocalization in these systems. These effects lead to a reduction in the HOMO–LUMO gap.

3. Conclusions

In conclusion, a new class of NIR emitting squarylium dyes **Sq1**–**3** has been synthesized, and the structural and electronic features were investigated using DFT methods. The high extinction coefficients, good quantum yields of fluorescence, and good photostability make these dyes suitable for application as fluorescent probes. The water compatibility and substantial enhancement of fluorescence of **Sq3** in micellar media suggest that these dyes can be potentially useful as fluorescent probes in biological applications where they can be used for imaging hydrophobic domains such as cell membranes, and such studies are currently being pursued.

4. Experimental

4.1. General

Squaric acid, 1-aminoanthracene, cetyltrimethylammonium bromide (CTAB), sodium dodecyl sulfate (SDS), and polyethylene-*tert*-octylphenol (Triton X-100) were purchased from Aldrich. All other starting materials and reagents were purchased from commercial suppliers and used without further purification. The solvents used were purified and dried by standard methods prior to use. Melting points were determined with a Mel-Temp-II melting point apparatus and are uncorrected. ^{1}H NMR spectra were measured on a 300 MHz Bruker Avance DPX and a 500 MHz Bruker Avance DRX spectrometer. FTIR spectra were recorded on a Shimadzu IRPrestige-21 Fourier Transform Infrared Spectrophotometer. High-resolution mass spectral (HRMS) analysis was obtained from JEOL JMS600 instrument. Electronic absorption spectra were recorded on a Shimadzu UV-3101 PC NIR scanning spectrophotometer and the emission spectra were recorded on a SPEX-Fluorolog, F112X spectrofluorimeter. Fluorescence lifetimes were measured using IBH (FluoroCube) time-correlated picosecond single photon counting (TCSPC) system using a 635 nm IBH NanoLED source and Hamamatsu C4878-02 MCP detector. The fluorescence decay profiles were deconvoluted using IBH data station software V2.1, fitted with monoexponential decay and minimizing the χ^2 values of the fit to 1±0.3. The solution phase geometries in ethanol were optimized for **DBAS**, **Sq1**, and **Sq2** at BLYP/6-31G* level of density functional theory in conjunction with the polarizable continuum (PCM) model of Tomasi and co-workers. The Gaussian 03 suite of programs was used for the calculations. The absorption properties of the systems optimized at BLYP/6-31G*-PCM level were further analyzed using the time-dependent DFT (TDDFT) calculations.

4.1.1. Synthesis of Sq1. A mixture of *N*,*N*-dimethyl-1-aminoanthracene (110 mg, 0.5 mmol) and squaric acid (28 mg, 0.25 mmol) was refluxed at 120 °C in a mixture of *n*-butanol (8 mL) and toluene (3.5 mL) for 12 h. The water formed during the reaction was distilled off azeotropically. After cooling, the reaction mixture was filtered and the residue was first purified by repeated precipitation from a mixture (1:4) of chloroform and hexane. The product was finally purified by recrystallization from chloroform to give the dye **Sq1** as a reddish brown solid.

Yield 78%; mp 265–267 °C (decomp.); FTIR (KBr): ν_{max} 1594 cm^{-1} (CO); UV λ_{max} (EtOH) 789 nm (ε 144,000 M^{-1} cm^{-1}); ^{1}H NMR (500 MHz, $CDCl_3$, TMS) δ 3.39 (12H, s, NCH_3), 7.00 (2H, d, J=8.6 Hz, aromatic C2 proton), 7.53 (2H, dd, J_1=7.4 Hz, J_2=7.0 Hz, aromatic C7 proton), 7.59 (2H, dd, J_1=7.0 Hz, J_2=7.3 Hz, aromatic C6 proton), 7.99 (2H, d, J=8.3 Hz, aromatic C8 proton), 8.34 (2H, d, J=8.3 Hz, aromatic C5 proton), 8.60 (2H, s, aromatic C9 proton), 9.57 (2H, d, J=8.6 Hz, aromatic C3 proton), 10.58 (2H, s, aromatic C10 proton); ^{13}C NMR (75 MHz, $CDCl_3$+TFA) δ 186.5, 178.0, 128.9, 123.0, 127.8, 121.9, 120.2, 118.8, 116.5, 112.7, 108.9, 47.7, 31.01. Mol. wt. calcd for $C_{36}H_{28}N_2O_2$ (MH^+): 520.2150; found (HRMS-FAB): 520.2131.

4.1.2. Synthesis of Sq2. A mixture of *N*,*N*-dimethyl aniline (10 mg, 0.08 mmol) and 3-[4-(*N*,*N*-dibutylamino)anthracene]-4-hydroxycyclobutene-1,2-dione (33.10 mg, 0.08 mmol) was heated at 60 °C in a mixture of tri-butylorthoformate (TBOF) (1 mL) and *n*-BuOH (10 mL) for 3 h. After cooling, the reaction mixture was filtered and the residue was purified by column chromatography over silica gel (100–200 mesh) as stationary phase and methanol/chloroform mixture (1:99) as eluant to give the dye **Sq2** as a pale reddish brown solid.

Yield 36%; mp 165–167 °C (decomp.); FTIR (KBr): ν_{max} 1596 cm^{-1} (CO); UV λ_{max} (EtOH) 720 nm (ε 70,000 M^{-1} cm^{-1}); ^1H NMR (300 MHz, $CDCl_3$, TMS) δ 0.95 (6H, t, aliphatic CH_3), 1.25–1.4 (4H, m, aliphatic CH_2), 1.68–2 (4H, m, aliphatic CH_2), 3.19 (6H, s, NCH_3), 3.64–3.68 (4H, t, NCH_2), 6.79 (2H, d, J=8.9 Hz, aromatic C13 and C15 protons), 6.99 (1H, d, J=8.7 Hz, aromatic C2 proton), 7.48–7.58 (2H, t, J=8.3 Hz, aromatic C6 and C7 protons), 7.95 (1H, d, J=7.9 Hz, aromatic C8 proton), 8.26 (1H, d, J=8.1 Hz, aromatic C5 proton), 8.5 (2H, d, J=8.4 Hz, aromatic C12 and C16 protons), 8.51 (1H, s, aromatic C9 proton), 9.42 (1H, d, J=8.6 Hz, aromatic C3 proton), 10.48 (1H, s, aromatic C10 proton); ^{13}C NMR (75 MHz, $CDCl_3$) δ 183.8, 160.2, 154.7, 137.2, 133.4, 132.9, 131.4, 130.8, 129.5, 128.5, 127.1, 126.4, 125.8, 125.2, 124.7, 120.3, 113.7, 112.6, 111.1, 110.0, 53.6, 40.5, 30.1, 29.9, 20.5, 14.0; (HRMS-FAB) Mol. wt. calcd for $C_{34}H_{36}N_2O_2$ (MH^+): 504.277; found: 504.2801.

4.1.3. Synthesis of Sq3. A mixture of *N*-phenyldiethanolamine (20 mg, 0.11 mmol) and 3-[4-(*N*,*N*-dimethylamino)-anthracene]-4-hydroxycyclobutene-1,2-dione (35 mg, 0.11 mmol) was heated at 60 °C in a mixture of tri-butylorthoformate (TBOF) (1 mL) and *n*-BuOH (10 mL) for 3 h. After cooling, the reaction mixture was filtered and the residue was purified by column chromatography over silica gel (100–200 mesh) as stationary phase and methanol/chloroform mixture (5:95) as eluant to give the dye **Sq3** as a green solid.

Yield 29%; mp 125–130 °C (decomp.); FTIR (KBr): ν_{max} 1590 cm^{-1} (CO); UV λ_{max} (EtOH) 720 nm (ε 34,000 M^{-1} cm^{-1}), ^1H NMR (300 MHz, CD_3OD, TMS) δ 3.47 (6H, s, NCH_3), 3.76 (4H, uneven triplet, J_1=5.7 Hz, J_2=5.2 Hz, $-CH_2OH$), 3.84 (4H, t, J=2.4 Hz, NCH_2), 6.92 (2H, d, J=8.9 Hz, aromatic C13 and C15 protons), 7.47–7.52 (2H, t, J=7.2 Hz, aromatic C6 and C7 protons), 7.54 (1H, d, J=9.1 Hz, aromatic C2 proton), 7.95 (1H, d, J=8.2 Hz, aromatic C8 proton), 8.12 (1H, d, J=8.3 Hz, aromatic C5 proton), 8.28 (2H, d, J=9.0 Hz, aromatic C12 and C16 protons), 8.53 (1H, s, aromatic C9 proton), 9.18 (1H, d, J=9.0 Hz, aromatic C3 proton), 10.12 (1H, s, aromatic C10 proton); ^{13}C NMR (75 MHz, CD_3OD) δ 178.0, 168.2, 167.4, 165.9, 140.2, 132.3, 129.3, 128.8, 126.5, 121.7, 119.0, 117.1, 114.2, 113.6, 113.1, 112.7, 112.4, 112.1, 111.6, 60.5, 60.3, 54.9, 30.9; (HRMS-FAB) Mol. wt. calcd for $C_{30}H_{28}N_2O_4$ (MH^+): 480.2049; found: 480.2037.

Acknowledgements

This work was financially supported by Department of Science and Technology (DST), Government of India, New Delhi and Council of Scientific and Industrial Research (CSIR, Task Force Program, COR-003). M.C.B., U.S., and S.A. thank CSIR, Government of India for research fellowships. This manuscript no. is RRLT-PPS-223.

Supplementary data

Some possible modes of addition of squaric acid to dimethyl aminoanthracene, ^1H NMR, ^1H–^1H COSY, and ^1H–^1H ROESY spectrum of **Sq1**, synthetic scheme for **Sq2** and **Sq3**, effect of surfactants (CTAB, Triton X-100) on absorption and fluorescence properties of squaraine dye **Sq3**, optimized geometries and energies of **DBAS**, **Sq1**, and **Sq2** at B3LYP/6-31G*-PCM method and MESP plotted onto the van der Waals' surface of **DBAS** and **Sq2**, Bader's AIM analysis data are available as Supplementary data. Supplementary data associated with this article can be found in the online version, at doi:10.1016/j.tet.2006.12.007.

References and notes

1. (a) Ye, Y.; Bloch, S.; Kao, J.; Achilefu, S. *Bioconjugate Chem.* **2005**, *16*, 51–61; (b) Ntziachristos, V.; Bremer, C.; Weissleder, R. *Eur. Radiol.* **2003**, *13*, 195–208; (c) Sevick-Muraca, E. M.; Houston, J. P.; Gurfinkel, M. *Curr. Opin. Chem. Biol.* **2002**, *6*, 642–650.
2. (a) Frangioni, J. V. *Curr. Opin. Chem. Biol.* **2003**, *7*, 626–634; (b) Pham, W.; Lai, W. F.; Weissleder, R.; Tung, C. H. *Bioconjugate Chem.* **2003**, *14*, 1048–1051.
3. (a) Das, S.; Thomas, K. G.; George, M. V. *Mol. Supramol. Photochem.* **1997**, *1*, 467–517; (b) Law, K.-Y. *Chem. Rev.* **1993**, *93*, 449–486.
4. (a) Stoll, R. S.; Severin, N.; Rabe, J. P.; Hecht, S. *Adv. Mater.* **2006**, *18*, 1271–1275; (b) Liang, K.; Farahat, M. S.; Perlstein, J.; Law, K.-Y.; Whitten, D. G. *J. Am. Chem. Soc.* **1997**, *119*, 830–831; (c) Das, S.; Thomas, K. G.; Kamat, P. V.; George, M. V. *J. Phys. Chem.* **1994**, *98*, 9291–9296; (d) Kamat, P. V.; Das, S.; Thomas, K. G.; George, M. V. *J. Phys. Chem.* **1992**, *96*, 195–199.
5. (a) Law, K.-Y.; Bailey, F. C. *J. Imaging Sci.* **1987**, *31*, 172–177; (b) Tam, A. C.; Balanson, R. D. *IBM J. Res. Develop.* **1982**, *26*, 186–197.
6. (a) Alex, S.; Santhosh, U.; Das, S. *J. Photochem. Photobiol., A* **2005**, *172*, 63–71; (b) Liang, K. N.; Law, K.-Y.; Whitten, D. G. *J. Phys. Chem.* **1995**, *99*, 16704–16708.
7. (a) Fabian, J.; Nakazumi, H.; Matsuoka, M. *Chem. Rev.* **1992**, *92*, 1197–1226; (b) Emmelius, M.; Pawlowski, G.; Volmann, H. W. *Angew. Chem., Int. Ed. Engl.* **1989**, *28*, 1445–1471.
8. (a) Basheer, M. C.; Alex, S.; Thomas, K. G.; Suresh, C. H.; Das, S. *Tetrahedron* **2006**, *62*, 605–610; (b) Ajayaghosh, A. *Acc. Chem. Res.* **2005**, *38*, 449–459; (c) Ros-Lis, J. V.; García, B.; Jiménez, D.; Martínez Máñez, R.; Sancenón, F.; Soto, J.; Gonzalvo, F.; Valldecabres, M. C. *J. Am. Chem. Soc.* **2004**, *126*, 4064–4065; (d) Yagi, S.; Fujie, Y.; Hyodo, Y.; Nakazumi, H. *Dyes Pigments* **2002**, *52*, 245–252; (e) Thomas, K. G.; Thomas, K. J.; Das, S.; George, M. V. *Chem. Commun.* **1997**, 597–598.
9. (a) Bello, K. A.; Corns, S. N.; Griffiths, J. *J. Chem. Soc., Chem. Commun.* **1993**, 452–453; (b) Sprenger, H. E.; Ziegenbein, W. *Angew. Chem., Int. Ed. Engl.* **1966**, *5*, 893–894.
10. Keil, D.; Hartmann, H.; Moschny, T. *Dyes Pigments* **1991**, *17*, 19–27.
11. Das, S.; Thomas, K. G.; Biju, P. V.; Santosh, U.; Suresh, V. U.S. Patent 6,417,402, 2002.
12. Law, K.-Y. *J. Phys. Chem.* **1989**, *93*, 5925–5930.
13. (a) Haugland, R. P. *Handbook of Fluorescent Probes and Research Chemicals*, 6th ed.; Molecular Probes: Eugene, OR, 1996; (b) Pham, W.; Medarova, Z.; Moore, A. *Bioconjugate Chem.* **2005**, *16*, 735–740; (c) Soper, S. A.; Mattingly, Q. L. *J. Am. Chem. Soc.* **1994**, *116*, 3744–3752.

14. Dempster, D. N.; Morrow, T.; Rankin, R.; Thompson, G. F. *J. Chem. Soc., Faraday Trans. 2* **1972**, *68*, 1479–1496.
15. (a) Das, S.; Thomas, K. G.; Thomas, K. J.; Madhavan, V.; Liu, D.; Kamat, P. V.; George, M. V. *J. Phys. Chem.* **1996**, *100*, 17310–17315; (b) Liang, K.; Law, K.-Y.; Whitten, D. G. *J. Phys. Chem.* **1994**, *98*, 13379–13384; (c) Chen, H.; Farahat, M. S.; Law, K.-Y.; Whitten, D. G. *J. Am. Chem. Soc.* **1996**, *118*, 2584–2594.
16. Das, S.; Thomas, K. G.; Ramanathan, R.; George, M. V.; Kamat, P. V. *J. Phys. Chem.* **1993**, *97*, 13625–13628.
17. Arun, K. T.; Ramaiah, D. *J. Phys. Chem. A* **2005**, *109*, 5571–5578.
18. (a) Jisha, V. S.; Arun, K. T.; Hariharan, M.; Ramaiah, D. *J. Am. Chem. Soc.* **2006**, *128*, 6024–6025; (b) Nizomov, N.; Ismailov, Z. F.; Nizamov, S. N.; Salakhitdinova, M. K.; Tatarets, A. L.; Patsenker, L. D.; Khodjayev, G. *J. Mol. Struct.* **2006**, *788*, 36–42; (c) Nakazumi, H.; Colyer, C. L.; Kaihara, K.; Yagi, S.; Hyodo, Y. *Chem. Lett.* **2003**, *32*, 804–805.
19. (a) Qu, J.; Müllen, K. *Angew. Chem., Int. Ed.* **2006**, *45*, 1401–1404; (b) Nakazumi, H.; Ohta, T.; Etoh, H.; Uno, T.; Colyer, C. L.; Hyodo, Y.; Yagi, S. *Synth. Met.* **2005**, *153*, 33–36; (c) Meier, H.; Petermann, R. *Helv. Chim. Acta* **2004**, *87*, 1109–1118; (d) Meier, H.; Petermann, R.; Gerold, J. *Chem. Commun.* **1999**, 977–978.
20. (a) Becke, A. D. *Phys. Rev. A* **1988**, *38*, 3098–3100; (b) Lee, C.; Yang, W.; Parr, R. G. *Phys. Rev. B* **1988**, *37*, 785–789.
21. Miertus, S.; Scrocco, E.; Tomasi, J. *J. Chem. Phys.* **1981**, *55*, 117–129.
22. Frisch, M. J., et al. *Gaussian 03, Revision C.02*; Gaussian: Wallingford, CT, 2004.
23. (a) Bader. *Atoms in Molecules: A Quantum Theory*; Oxford University Press: Oxford, 1990; (b) Biegler-Konig, F.; Schonbohm, J.; Derdau, R.; Bayles, D.; Bader, R. F. W. *AIM2000; Version 1*; Bielefeld, Germany, 2000.
24. MESP is directly related with the electron density distribution and the most negative-valued MESP is often observed at the electron rich regions such as lone pair and π-bonded regions of a molecule or more on MESP, see: (a) Politzer, P.; Truhlar, D. G. *Chemical Applications of Atomic and Molecular Electrostatic Potentials*; Plenum: New York, NY, 1981; (b) Gadre, S. R.; Shirsat, R. N. *Electrostatics of Atoms and Molecules*; Universities Press: Hyderabad, 2000.
25. (a) Suresh, C. H.; Gadre, S. R. *J. Org. Chem.* **1999**, *64*, 2505–2512; (b) Suresh, C. H.; Gadre, S. R. *J. Am. Chem. Soc.* **1998**, *120*, 7049–7055; (c) Suresh, C. H.; Koga, N. *Inorg. Chem.* **2002**, *41*, 1573–1578.
26. Stratmann, R. E.; Scuseria, G. E.; Frisch, M. J. *J. Chem. Phys.* **1998**, *109*, 8218–8224.